Data analysis to assess part quality in DED-LB/M based on in-situ process monitoring

Pilar Rey, Camilo Prieto, Carlos González, Konstantinos Tzimanis, Thanassis Souflas, Panagiotis Stavropoulos, Jitendra-Singh Rathore, Vincent Bergeaud, Caroline Vienne, Philippe Bredif

12th CIRP Conference on Photonic Technologies [LANE 2022], 4-8 September 2022, Fürth, Germany

Data analysis to assess part quality in DED-LB/M based on in-situ process monitoring

Pilar Rey[a],*, Camilo Prieto[a], Carlos González[a], Konstantinos Tzimanis[b], Thanassis Souflas[b], Panagiotis Stavropoulos[b], Jitendra Singh Rathore[c], Vincent Bergeaud[c], Caroline Vienne[c], Philippe Bredif[c]

[a]AIMEN Technology Centre, Polígono Industrial de Cataboi SUR-PPI-2 (Sector) 2, Parcela 3, O Porriño, E36418, Spain
[b]Laboratory for Manufacturing Systems and Automation (LMS), University of Patras, Rio, Patras 26504, Greece
[c]Université Paris-Saclay, CEA, LIST, F-91190, Palaiseau, France

* Corresponding author. Tel.: +34 986 344 000; E-mail address: prey@aimen.es

Abstract

In the field of Laser beam Direct Energy Deposition (DED-LB/M) for metal additive manufacturing, the implementation of qualification strategies parts from monitoring data and reduced order models is presently at low level of maturity. In this work, a methodology and a suite of novel data analysis tools targeting the joint analysis of multimodal data: process parameters, coaxial thermal imaging and part quality by Computer Tomography scans is presented. To demonstrate the proposed approach, a set of stainless-steel coupons were built with varying process parameters (power, process speed) and path planning strategies. Exploratory data analysis and feature engineering was performed on the dataset: process indicators, thermal and geometrical monitoring features are correlated to spatially resolved defects (mainly cracks) as well as the overall part quality obtained from the inspection phase paving the way for further implementation of in-situ process monitoring as a reliable tool for process optimization and qualification.

Keywords: in-situ monitoring; Direct Energy Deposition; Additive Manufacturing; data analytics; part quality

1. Introduction

Direct Energy Deposition (DED) processes are showing a growing interest in the industry as they have strong capabilities to build large-sized and complex or customized parts, produce multi-material items and clad/repair pre-existing metallic damaged valuable components. Qualification of DED-LB/M process includes many different aspects such as part design, feedstock material, process parametrization and process planning, with the geometry, laser power, scanning speed and material flow rate being the most influential for achieving part quality. Additionally, temporal history in terms of heating and cooling rates has a significant influence on part properties and potential defects such as cracks [1-3].

One significant approach that has concentrated the efforts of the research community to overcome this complexity is by process monitoring combined with real time close loop control and in-situ process characterization [4][5] In [6] a method to visualize thermal metrics during DED-LB/M process to evaluate thermally driven and material features was introduced.

In this paper a novel data analysis methodology is presented to study relationships between the AM process parameters and the part quality characteristics using real-time process monitoring and NDT inspection. The corresponding process, monitoring and inspection data gathered to capture and analyze the relevant real-time physics of the process will be comprehensively detailed. Results on the analysis of relevant

process features related to process information and part quality metrics is elaborated.

2. Experimental Procedure

2.1. DED-LB/M manufacturing and NDT inspection

Stainless steel SS316L powder (Flame Spray Tech, Particle Size Distribution: 45-105 µm) and 316L base plates of 10 mm of thickness were used to manufacture several single-wall coupons using different laser process parameters and scanning strategies (Table 1 & Fig.1.)

This work is part of a bigger one in which additionally other DED manufacturing process and feedstock with no defect promotion were investigated, dataset available in this open repository [7,8]. The data analysis presented in this paper refers only to the coupons were most of the defects have been found, namely Cc_7, Cc_8, Cc10, Cc_11, Cc_12, Cc_13.

Table 1. Process parameters

Cc coupon	Laser Power (W)	Scanning Speed (mm/s)	Strategy
Cc_7	850	6	1
Cc_8	650	10	1
Cc_10	850	6	2
Cc_11	650	10	2
Cc_12	850	6	3
Cc_13	850	6	4

Laser beam spot diameter was set at 2mm and the powder flow at 8g/min, using argon as carrier and protective gas. The different set of process parameters (speed/power) determine the energy density (2) and finally the produced track height and width. By providing less energy density, the track dimensions become narrower compared to that manufactured with higher energy density.

Therefore, when less energy is provided, more layers are required in order to achieve the same height. For instance, in Cc_7, Cc_10, Cc_12, Cc13, the produced layer height is 0.70mm while in Cc_8, Cc_11 the layer height is $0.46\ mm$ and the total part height in all cases is $50\ mm$.
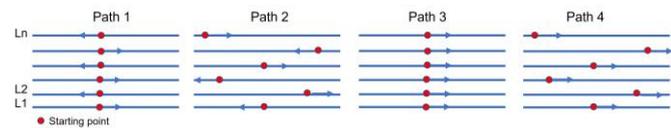

Fig. 1. Path strategies evaluated (Ln: layer number).

Manufacturing workstation used consisted of a 6 axes ABB IRB4400 robot, a 15kW TruDisk laser (TRUMPF), a laser head, BEO D70 (TRUMPF) with a coaxial nozzle COAX 8 (FHG-IWS) and powder feeder (MEDICOAT) Coaxial thermal

images were registered by a 64x64pixel 12bits MWIR Tachyon sensor (NIT) and four thermocouples soldered to the base plate were set at fixed position for all tests (Fig. 2.).
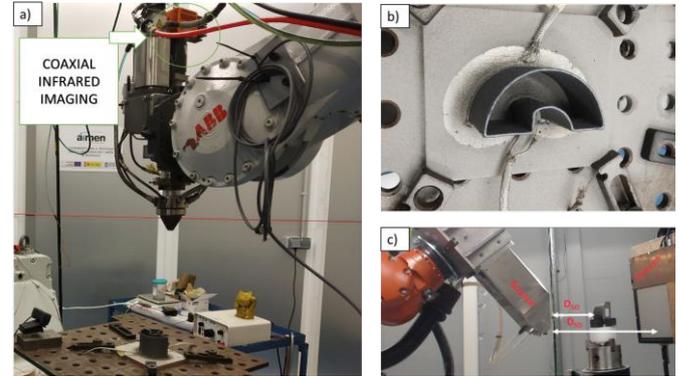

Fig. 2. (a) Set up for manufacturing and coaxial imaging process observation; (b) top view of coupon part as built with termocouples attached; (c) robotized CT-scan system at CEA list.

A robotized X-ray tomography micro-focus system (Fig. 2c) was used for the NDT inspection with an optimised set of parameter settings (namely: Voltage: 220 kV, Current, 220 µA, 900 projections) achieving voxel size of 105µm. The post-processing of the tomography acquisition was performed in VGStudioMax 3.5 software (Volume Graphics). It provides the dedicated modules for flaw identification and quantitative information related to defects. Information to align and register CT data with CAD and other data sources can also be extracted from this software.

Datasets of the build and monitoring information of the Cc coupons were collected at the acquisition rate of 10Hz during process execution in hdf5 file format (in-house developed software by AIMEN: Capturer). From coaxial images registered, geometrical and thermal features implementing image processing algorithms are evaluated and visualized in 3D (in-house developed software by AIMEN: 3Dinspector) [8, 9]. A large set of features is calculated by using different regions of the process interaction area: meltpool, tail, and Heat Affected Zone (HAZ) as shown in Fig. 3.
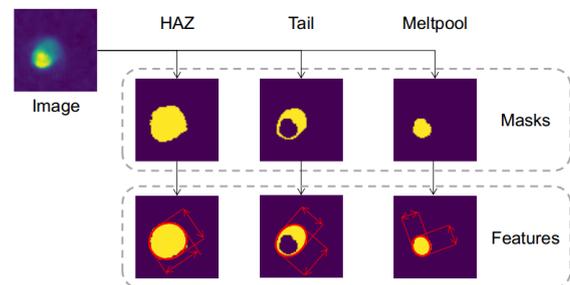

Fig. 3. Feature extraction and process regions segmentation.

Each one of the features is affected in a specific way with different combinations of speed and power [10]. With constant power, when the deposition speed increases, larger length

features are expected while when the deposition speed decreases wider width features are expected. The direction of heat conduction and the heat losses on width and length axes determine the way that each feature is affected every time that speed and power parameters change. Moreover, in the case where the width of the part equals the laser spot diameter (single wall structure), it is better to study directly the HAZ features since the melt pool region, can not be isolated very well from the rest regions, considering high heat accumulation in very small area. This can lead to obtain misleading outputs from the sensing devices. Considering that coupons as single wall structures, the HAZ features will be studied in this work instead of the melt pool features which are usually corelated with process inputs in similar studies. [11,12].

2.2. Data analytics

Energy related metrics and indicators based on the dimensions of the HAZ features (width, length, area) are calculated dynamically with inputs from process data with the following equations (1-5), giving an insight on how the data trend change across the height of the part. The symbols that are used for the calculation of the metrics are described hereafter. SE is used for specific energy, the ED for energy density while the CR and FN for cooling rate and Fourier number accordingly. The latter is a dimensionless number. P is used for laser power, u for deposition speed, lt for layer thickness, A for laser absorption, ρ for material density, Cp for specific heat capacity, k for thermal conductivity, and EI for energy input, mw, ml and ms originally, are used for melt pool width, length and size, however, in this case are used for HAZ diameter, HAZ length and HAZ area accordingly. These metrics can apply for all the regions that described in Fig. 3 by using the related features such as tail width, tail length and tail area where the width, length and area dimensions are required.

$$SE (J/m^2) = \frac{P}{u \times mw} \quad (1)$$

$$ED \left(\frac{J}{m^3}\right) = \frac{P}{u \times mw \times lt} \quad (2)$$

$$CR\ (°C/sec) = \frac{A \times P \times u^{1/2}}{mw^{\frac{5}{2}} \times (2\rho \times C_p \times k)^{1/2}} \quad (3)$$

$$FN = \frac{\frac{k}{\rho \times C_p}}{u \times ml} \quad (4)$$

$$EI \left(\frac{J}{m}\right) = ED \times ms \quad (5)$$

Based on the process parameters of the different coupons, described in Table 1, the values of specific energy (SE), energy density (ED) and energy input (EI) are calculated and included in Table 2. The mw is considered before the beginning of the processes equal to the laser spot diameter and the ms is

calculated considering the area that is covered from the laser beam. Originnaly, these values are calculated so as to indicate the provided energy and to compare later the end-products dimensions and quality based on these values. In addition, instead of mw, in non single wall structures, the hatching distance or the bead width can be used for the calculation of energy related metrics [13]. However, as it can be seen on the following experimental results, the dimensions of mw can deviate significantly from the laser spot diameter due to the described effect of different process parameters on the heat dissipation and heat loss.

Table 2. Energy related metrics.

Cc coupon	Specific Energy (J/m^2)	Energy Density (J/m^3)	Energy Input (J/m)
Cc_7	70.83	101.19	350.31
Cc_8	32.50	70.65	244.59
Cc_10	70.83	101.19	350.31
Cc_11	32.50	70.65	244.59
Cc_12	70.83	101.19	350.31
Cc_13	70.83	101.19	350.31

Similarly, the Fourier Number (4) and the Cooling Rate (3) were calculated and used as input of the exploratory data analysis performed. During the process, the HAZ geometrical features deviate, and analogously for the described metrics.

At the initial phase of the data analysis, the quality of the acquired data is validated by interpretating the data trends with the physic-based indicators and process related rules. Then, the correlation of data channels from monitoring devices with metrics that are related to the defect inspection was investigated (e.g., number of cracks across the different layers). The labelled data from NDT and process data are registered on common coordinate system so as to improve the mapping of cracks on the CAD and the detection of defects on the path planning trajectories of manufactured parts. The methodology and approach are included in Fig. 4.
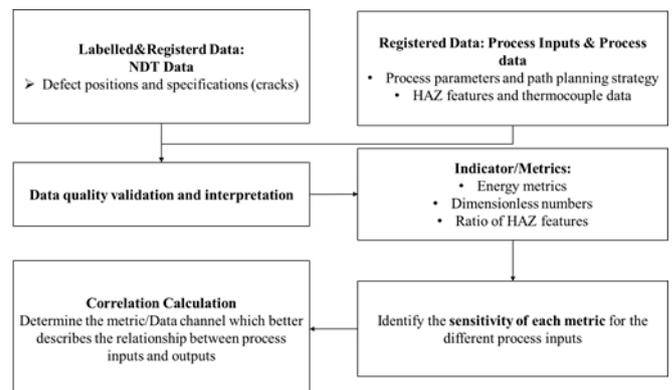

Fig. 4. Workflow for data analytics and correlation of process inputs with outputs.

3. Results and Discussion

3.1. Part quality:3D monitoring and inspection visualization

At first stage, by visual inspection, it is clearly noted the geometrical accuracy and final finish quality together with crack defects are dependent on the laser parameters and the scanning strategy used. Cc_12 present cracks from the first layer together with a strong defect on the center seam due to high heat accumulation compared with Cc7. Cc_8 presents visually more cracks than Cc_7 due to a faster cooling (Fig. 5.).

The 3D reconstruction with the thermal features of the melt pool provides additional information (Fig. 6.) that Cc coupons becomes hotter as they grow in the Z direction, being this related with the heat dissipation mechanisms across the height. Also, laser start- stop is easily recognized promoting a noticeable seam on the central part of the coupons with strategy 1 and 3. Finally, the effect of energy density Cc_7 VS Cc_8 can be appreciated in the emissivity thermal feature of the melt pool.
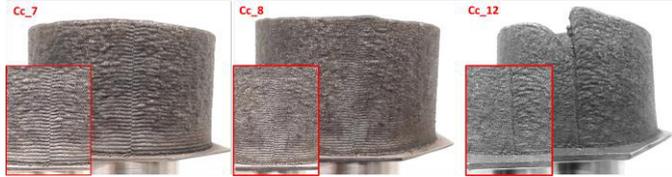
Fig. 5. Visual aspect of Cc_7, 8 &12 showing a detail on the centre part of the coupons.
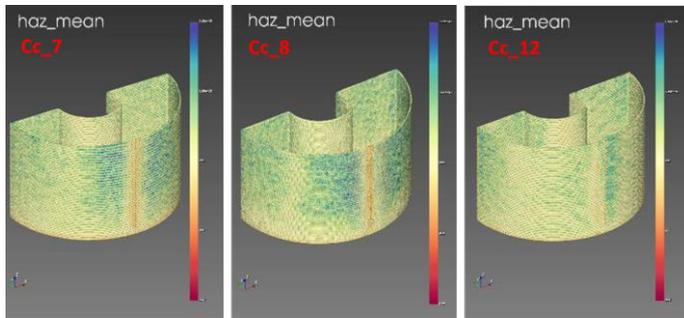
Fig. 6. 3D thermal reconstruction for Cc_7, 8 & 12

The Fig. 7. presents the 3D visualization of the coupons with the defect quantification and distribution in the volume. Table 3 shows the quantitative metrics extracted from the CT scan analysis [14]. In those, influence of process parameters and path planning in the generation of defects of the different Cc_coupons is presented. More cracks are present in Cc_8 and CC_11 compared with Cc_7 and Cc_10 due to different energy density. Also, differences due to the path planning in that coupons were observed. Additionally, Cc_12 seams to present less but bigger cracks, starting from the first layers as in the CC_13 case. This can be related with the different thermal gradients, as the originated by the different path planning, in which all the tracks go through the same direction.
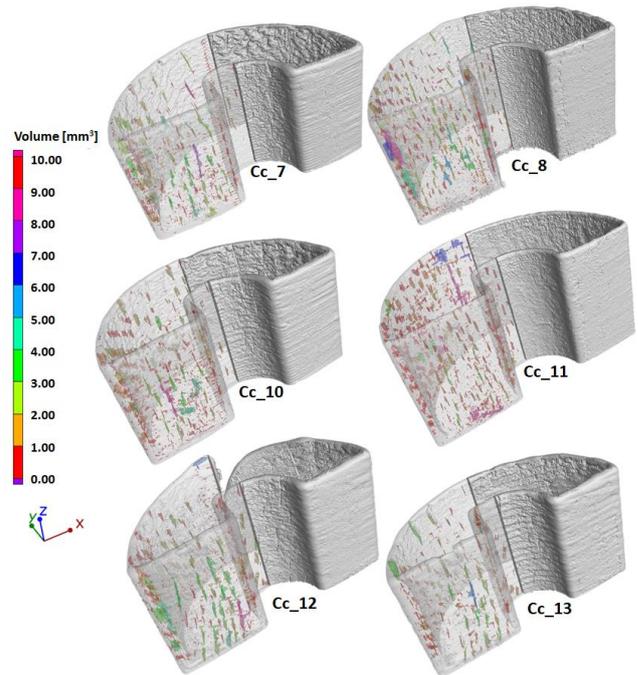
Fig. 7. Tomography results with detection of crack in the coupons (the color bar represents the size of the crack/defect in terms of volume) the total defect volume and the defect volume ratio is reported for each coupon

Table 3. CT scan data analysis

Cc coupon	Defect vol (mm³)	Material vol (mm³)	Defect vol. ratio (%)
Cc_7	399,06	32117,99	1,23
Cc_8	575,38	25508,76	2,21
Cc_10	447,97	30465,84	1,45
Cc_11	577,09	24350,36	2,32
Cc_12	685,54	35218,39	1,91
Cc_13	379,71	34359,69	1,09

3.2. Exploratory data analysis

The first step of the analysis is to investigate the quality of the provided datasets as well as to reach some initial conclusions about the data trends. To do that, the layer per layer analysis where all the information for a specific layer has been gathered aiming to calculate the mean value and variance of each data channel, indicator, and metric for the respective layer was used. This step will give a better understanding related to the way that the monitored features alter across the height of the part.

For HAZ dimensions monitoring, physics-based rules are satisfied. First, small HAZ dimensions are detected near to the substrate material due to the significant thermal gradients,

considering the temperature of the substrate material constant and equal to 30℃ (Fig. 8.a). With increasing deposition height, the HAZ dimensions grow due to more uniform temperature to the previously deposited layers and after, almost, twenty (20) layers (0.7 mm layer height) for Cc_7, Cc_10, Cc_12, Cc13 and thirty (30) layers (0.46 mm layer height) for Cc_8, Cc_11 the dimensions remain constant (Fig. 8.b). This is equivalent to around 14mm distance from the base plate in all coupons. Moreover, the HAZ features seem to be affected from the different combination of process parameters. As an example, by reducing provided energy density, smaller features are detected while by rising the deposition speed, the length features grow with higher rate than width. The opposite is noticed, with reduced speed, where the width feature grows faster than length (Fig. 8b). These outputs can be explained by considering the effect of deposition speed on the heat loss due to conduction [11,12]. Finally, repeatable trends are obtained when similar process parameters are used (Fig. 8.c).
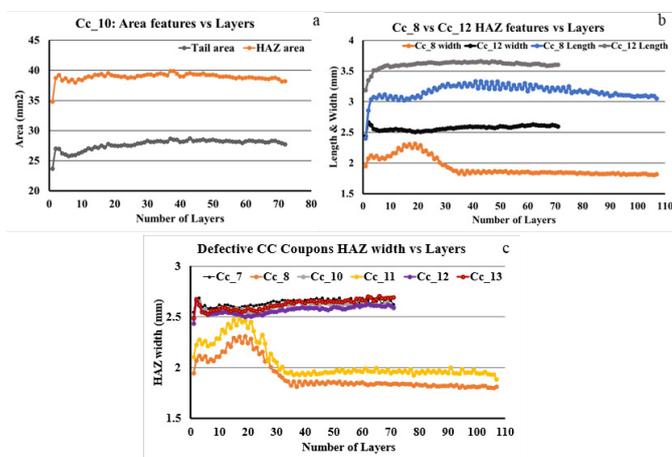

Fig. 8. HAZ geometrical features vs number of layers

In addition, the data from thermocouples which are placed on the bottom of the part (2), depicts the effect of the tested path planning strategies and process parameters on the heat accumulation and on the thermal gradients, as it can be seen in Fig. 9. a & c. The different thermal gradients can be justified also from the reduced energy density (2) in Cc_8, compared to Cc_12. Additionally, when the thermal gradients become minimal the HAZ dimensions deviation gets minimum which ensure the consistency between data from different sources (Fig. 9). On the same direction, maximum thermal gradients are obtained at the initial layers, when the temperature difference with the substrate is huge while repeatability of trends is met once again. By taking advantage of the transformation matrices for the CT scan data and by mapping the defects on each layer, how the trend of defects changes with the distance from the substrate material (Fig. 9.) can be seen.

The high number of cracks at the initial layers (Fig. 10.) can be justified considering the huge thermal gradients that can lead to high thermal stresses and finally cracking [4,12]. To this end,

the number of cracks per layer is utilized as metric so as to investigate the correlation of data channels with the detected defects on process outputs.
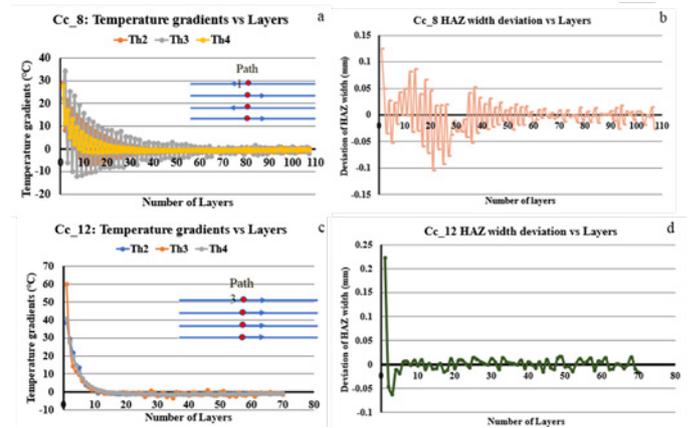

Fig. 9. Simultaneous analysis of HAZ features dimensions and thermocouple data for Cc_8 (a, b), Cc_12 (c, d)
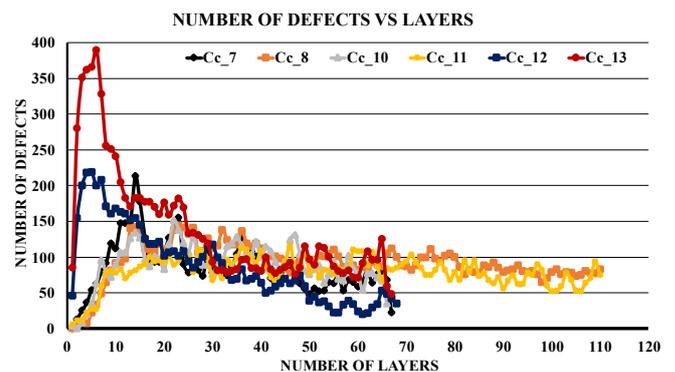

Fig. 10. Number of cracks vs number of layers

The Pearson correlation coefficient is used to point which data channel and metrics can be correlated stronger with the number of cracks per layers. By calculating the coefficient for the different coupons, as well as for all the coupons together, it was found that the HAZ area, HAZ width, Fourier number (4) and the Energy Input (5), can be correlated stronger (coefficient>0.8) with the defects per layer, considering HAZ features from monitoring devices. The strong correlation indicates that the aforementioned datasets incorporate information that can be used to evaluate the process performance and detection of defects when specific rules (process or physics-based) are satisfied. Thus, meaning that these channels are potentially to be considered as predictors for the development of predictive machine learning models that detect defects based on the obtained values from sensing devices and the calculation of the energy related metrics. To develop/train such models, a wider experimental campaign is required.

4. Conclusions

The combined data from thermocouples and HAZ monitoring has given an overview about how different process parameters and path planning strategies affect the HAZ geometrical features and the heat accumulation. Thus, being those important for the DED-LB/M process mechanism, the correlation of process metrics and indicators with NDT data can be used for future in line applications of the generated knowledge.

Additionally, by comparing results from NDT with the selected process inputs it can be found that higher defect density is found in Cc coupons where the achieved HAZ dimensions are smaller (lower energy density), favoring the development of cracks due to high thermal stresses promoted during manufacturing. On the other hand, path planning strategy has also an strong influence in samples even with the same energy density. Some path planning strategies can create large heat accumulation on the part promoting severe defects as overmelting and also, with the end of the process, cracks can be formed considering the high cooling rate.

Furthermore, it can be extracted from the presented results that in cases where path planning strategies 1,2 were selected, the temperature gradients are larger, creating the circumstances for heat cycles that are not desired during manufacturing (thermal stresses), while also the HAZ dimensions stabilized with slower rate compared to the cases where the path planning strategies 3.4 were selected.

Acknowledgements

References

[1] Thompson, S. M., Bian, L., Shamsaei, N., & Yadollahi, A. (2015). An overview of Direct Laser Deposition for additive manufacturing; Part I: Transport phenomena, modeling and diagnostics. Addit. Manuf., 8, 36-62.

[2] Shamsaei, N., Yadollahi, A., Bian, L., & Thompson, S. M. (2015). An overview of Direct Laser Deposition for additive manufacturing; Part II: Mechanical behavior, process parameter optimization and control.Addit. Manuf., 8, 12-35.

[3] Kim, F. H., Kim, F. H., & Moylan, S. P. (2018). Literature review of metal additive manufacturing defects (pp. 100-16). Gaithersburg, MD, USA: US Department of Commerce, National Institute of Standards and Technology.

[4] He, W., Shi, W., Li, J., & Xie, H. (2019). In-situ monitoring and deformation characterization by optical techniques; part I: Laser-aided direct metal deposition for additive manufacturing. Optics and Lasers in Engineering, 122, 74-88.

[5] Everton, S. K., Hirsch, M., Stravroulakis, P., Leach, R. K., & Clare, A. T. (2016). Review of in-situ process monitoring and in-situ metrology for metal additive manufacturing.Materials & Design, 95, 431-445.

[6] Kriczky, D. A., Irwin, J., Reutzel, E. W., Michaleris, P., Nassar, A. R., & Craig, J. (2015). 3D spatial reconstruction of thermal characteristics in directed energy deposition through optical thermal imaging. J. Mat. Proc. Tech., 221, 172-186.

[7] Prieto, C., Gonzalez, C., Carracelas, S. Lodeiro, B., Arias, J., 3D thermal mapping during AM by LMD towards better part quality. Proceedings Lasers in Manufacturing 2019

[8] https://zenodo.org/record/5031586#.YZZhxtDMJPZ.

[9] Carlos González Val, Roberto Fernández Molanes, & Baltasar Lodeiro Señarís. (2021). Visualizer (3.0.1). Zenodo. https://doi.org/10.5281/zenodo.5469946

[10] Sammons PM. Height dependent laser metal deposition process modelling Master's Thesis, Misouri University of Science and Technology, 2015; https://scholarsmine.mst.edu/masters_theses/7446

[11] Rao PK, Liu JD, Kong Z, Williams C. Online Real-Time Quality Monitoring in Additive Manufacturing Processes Using Heterogeneous Sensors, J. Manuf. Sci. Eng. 2015; 137(6).

[12] Ocylok S, Alexeev E, Mann S, Weisheit A, Wissenbach K, Kelbassa I, . Correlations of Melt Pool Geometry and Process Parameters During Laser Metal Deposition by Coaxial Process Monitoring. Physics Procedia. 56. .2014; 228–238. 10.1016/j.phpro.2014.08.167.

[13] E. R. Lois, R. F. Molanes, C. González-Val, J. J. Rodríguez-Andina and J. Fariña, "Online Calculation of Melt Pool Cooling Rate with Automatic Background Correction," IECON 2019 - 45th Annual Conference of the IEEE Industrial Electronics Society, 2019, pp. 3085-3090, doi: 10.1109/IECON.2019.8927062.CEA

[14] Rathore, J.S., Vienne, C., Quinsat, Y. *et al.* Influence of resolution on the X-ray CT-based measurements of metallic AM lattice structures. *Weld World* **64,** 1367–1376 (2020). https://doi.org/10.1007/s40194-020-00920-4